Camassa-Holm Equations as a Closure Model for Turbulent Channel and Pipe Flow

Shiyi Chen,[1] Ciprian Foias,[1,2] Darryl D. Holm,[1] Eric Olson,[1,2] Edriss S. Titi,[3,4,5] and Shannon Wynne[3,5]
[1]*Theoretical Division and Center for Nonlinear Studies, Los Alamos National Laboratory, Los Alamos, New Mexico 87545*
[2]*Department of Mathematics, Indiana University, Bloomington, Indiana 47405*
[3]*Department of Mathematics, University of California, Irvine, California 92697*
[4]*Department of Mechanical and Aerospace Engineering, University of California, Irvine, California 92697*
[5]*Institute for Geophysics and Planetary Physics, Los Alamos National Laboratory, Los Alamos, New Mexico 87545*
(Received 15 April 1998; revised manuscript received 9 September 1998)

We propose the viscous Camassa-Holm equations as a closure approximation for the Reynolds-averaged equations of the incompressible Navier-Stokes fluid. This approximation is tested on turbulent channel and pipe flows with steady mean. Analytical solutions for the mean velocity and the Reynolds shear stress are consistent with experiments in most of the flow region. [S0031-9007(98)07958-7]

PACS numbers: 47.60.+i, 47.27.–i

Laminar Poiseuille flow occurs when a fluid in a straight channel, or pipe, is driven by a constant upstream pressure gradient, yielding a symmetric parabolic streamwise velocity profile. In turbulent states, the mean streamwise velocity profile remains symmetric, but is flattened in the center because of the increase in velocity fluctuations. A lot of research has been carried out for turbulent channel flow, e.g., Refs. [1–6]; however, accurate measurement of the mean velocity and the Reynolds stress profiles, in particular for flows at high Reynolds numbers, is still an experimental challenge. In the case of pipe flow, recent experiments for measuring the mean-velocity profile have been successfully performed at moderate to high Reynolds numbers [7]. However, the fundamental understanding of how these profiles change as functions of the Reynolds number is still missing.

In wall bounded flows it is customary to define a characteristic velocity u_* and Reynolds number R_0 by $u_* = \sqrt{|\tau_0|/\rho}$ and $R_0 = du_*/\nu$, where τ_0 is the boundary shear stress, density ρ is unity, ν is the molecular viscosity of the fluid, and d is a characteristic macrolength. For instance, the channel half-width is d in channel flow, and the pipe radius is d in pipe flow. Based on experimental observation and numerical simulation, a piecewise expression of the mean velocity across the channel has been commonly accepted [8], for which the nondimensional mean streamwise velocity, $\phi \equiv U/u_*$, is assumed to depend on $\eta \equiv u_*\delta/\nu$ and have three types of behavior, depending on the distance away from the wall boundary δ: a viscous sublayer, in which $\phi \sim \eta$; the von Kármán logarithmic "law of the wall," in which $\phi(\eta) = \kappa^{-1} \ln \eta + A$, where $\kappa \simeq 0.41$ and $A \simeq 5.5$; and a power law region, in which $\phi \sim \eta^p$, $0 < p < 1$. Alternatively, in [9] a single curve fitting over the whole region is proposed. Yet another proposal [10] is a family of power laws that fit the data away from the viscous sublayer, and has the log law as an envelope.

In this paper we propose the viscous Camassa-Holm equations (VCHE) [in Eq. (4)] as a closure approximation for the Reynolds equations. Our primary aim is to illustrate the connection between turbulence and the VCHE. The analytic form of our profiles based on the steady VCHE applies away from the viscous sublayer (but encompassing at least 95% of the flow region) and depends on two free parameters: the flux Reynolds number $R = d\overline{u}/\nu$ (where $\overline{u}$ is the mean flux) and R_0. Because of measurement limitations, most experimental data are contained in this region. Let us remark that we can further reduce the parameter dependence to one free parameter by using a prescribed drag law for the wall friction defined by $D = 2R_0^2/R^2$. For the remaining wall region of the flow, we are unable to determine the mean profile explicitly without further assumptions. However, we can show compatibility of the steady VCHE with empirical and numerical velocity profiles in the near-wall region [11]. The VCHE profiles are consistent with data obtained from turbulent channel and pipe flow measurements and simulations.

We begin our theoretical treatment by recalling the Reynolds-averaged Navier-Stokes equations [8,12]:

$$\frac{\partial\langle\mathbf{u}\rangle}{\partial t} + \langle\mathbf{u}\rangle \cdot \nabla\langle\mathbf{u}\rangle = \mathrm{div}\langle\mathbf{T}\rangle, \qquad \mathrm{div}\langle\mathbf{u}\rangle = 0\,, \quad (1)$$

where $\langle\cdot\rangle$ denotes the ensemble average and $\langle\mathbf{T}\rangle = -\langle p\rangle\mathbf{I} - \langle\mathbf{u}\otimes\mathbf{u}\rangle + \nu(\nabla\langle\mathbf{u}\rangle + \nabla\langle\mathbf{u}\rangle^T)$. Our approach holds for both the channel and the pipe flows; however, for brevity we will give details only for the channel case. For turbulent channel flow, the mean velocity is of the form $\langle\mathbf{u}\rangle = [\overline{U}(z), 0, 0]^T$, with $\langle p\rangle = \overline{P}(x, y, z)$ and the Reynolds equations (1) reduce to $\mathrm{div}\langle\mathbf{T}\rangle = 0$, or equivalently,

$$\begin{aligned} -\nu\overline{U}'' + \partial_z\langle wu\rangle &= -\partial_x\overline{P}\,, \\ \partial_z\langle wv\rangle = -\partial_y\overline{P}, \qquad \partial_z\langle w^2\rangle &= -\partial_z\overline{P}\,, \end{aligned} \quad (2)$$

where $(u, v, w)^T$ is the fluctuation velocity in the infinite channel $\{(x, y, z) \in \mathbb{R}^3, -d \le z \le d\}$. The $(1, 3)$ component of the averaged stress tensor $\langle\mathbf{T}\rangle$ is given by

 0031-9007/98/81(24)/5338(4)$15.00

$\langle T_{13}\rangle = -\nu\overline{U}'(z) + \langle wu\rangle$. On the boundary, the velocity components all vanish and one has the stress condition

$$\mp\tau_0 = \langle T_{13}\rangle|_{z=\pm d} = \nu\overline{U}'(z)|_{z=\pm d}\,, \tag{3}$$

upon using $\langle wu\rangle = 0$ at $z = \pm d$. Hence, the Reynolds equations imply $\langle w\boldsymbol{v}\rangle(z) \equiv 0$ and $\overline{P} = P_0 - \tau_0 x/d - \langle w^2\rangle(z)$, with integration constant P_0.

The VCHE are

$$\frac{d\mathbf{v}}{dt} + v_j\nabla u^j + \nabla\pi = \nu\nabla^2\mathbf{v}, \qquad \nabla\cdot\mathbf{u} = 0\,, \tag{4}$$

where $\mathbf{v} = [\mathbf{I} - (\nabla\cdot\langle\sigma\rangle)]\mathbf{u} - \partial_i(\langle\sigma_i\sigma_j\rangle\partial_j\mathbf{u})$, the material derivative $d/dt = \partial/\partial t + \mathbf{u}\cdot\nabla$, and π is the modified pressure, $\pi = p - 1/2|u|^2 - 1/2\langle\sigma_i\sigma_j\rangle\mathbf{u}_{,i}\mathbf{u}_{,j}$, where p is the usual pressure. In Ref. [13], Eq. (4) with $\nu = 0$ is derived by decomposing Lagrangian parcel trajectories into mean and fluctuating parts as $\mathbf{X}^\sigma(\mathbf{a},t) = \mathbf{X}(\mathbf{a},t) + \sigma[\mathbf{X}(\mathbf{a},t),t]$ and assuming isotropy and homogeneity of the fluctuations σ with components σ_i, $i = 1$, 2, and 3. Isotropy implies $\langle\sigma_i\sigma_j\rangle = \alpha^2\delta_{ij}$ with $\langle\sigma\rangle = 0$, where α is a local length scale. Homogeneity, in addition to isotropy, implies that α is constant. This derivation generalizes a one-dimensional integrable dispersive shallow water model studied in [14] to n dimensions and provides the interpretation of α as the typical mean amplitude of the fluctuations. Thus, it is clear that the solutions of VCHE are mean quantities.

Before comparing VCHE with Reynolds averaged equations, we rewrite Eq. (4) (with α constant) in the equivalent constitutive form,

$$\frac{d\mathbf{u}}{dt} = \operatorname{div}\mathbf{T}, \qquad \mathbf{T} = -p\mathbf{I} + 2\nu(\mathbf{I} - \alpha^2\nabla^2)\mathbf{D} + 2\alpha^2\dot{\mathbf{D}}\,, \tag{5}$$

with $\nabla\cdot\mathbf{u} = 0$, $\mathbf{D} = (1/2)(\nabla\mathbf{u} + \nabla\mathbf{u}^T)$, $\Omega = (1/2)(\nabla\mathbf{u} - \nabla\mathbf{u}^T)$, and corotational (Jaumann) derivative given by $\dot{\mathbf{D}} = d\mathbf{D}/dt + \mathbf{D}\Omega - \Omega\mathbf{D}$. In this form, one recognizes the constitutive relation for VCHE as a variant of the rate-dependent incompressible homogeneous fluid of second grade [15,16], whose viscous dissipation, however, is modified by the Helmholtz operator $(\mathbf{I} - \alpha^2\nabla^2)$. There is a tradition, at least since Rivlin [17], of modeling turbulence by using continuum mechanics principles, such as objectivity and material frame indifference (see also Ref. [18]). For example, this type of approach is taken in deriving Reynolds stress algebraic equation models [19]. Rate-dependent closure models of mean turbulence have also been obtained by the two-scale direct-interaction approximation approach [20] and by the renormalization group method [21]. Since VCHE describe mean quantities, we propose to use (4) as a turbulence closure model and test this ansatz by applying it to turbulent channel and pipe flows.

In the case of channel flow, we denote the velocity $\mathbf{u}$ in (4) by $\mathbf{U}$ and seek its steady state solutions in the form $\mathbf{U} = [U(z),0,0]^T$ subject to the boundary condition $U(\pm d) = 0$ and the symmetry condition $U(z) = U(-z)$. In this particular case, the steady VCHE reduces to

$$\begin{aligned} -\nu[(1-\beta')U]'' + \nu(\alpha^2U')''' &= -\partial_x\tilde{\pi}\,, \\ 0 = -\partial_y\tilde{\pi}, \qquad 0 &= -\partial_z\tilde{\pi}\,. \end{aligned} \tag{6}$$

Here $\alpha^2 = \langle\sigma_3^2\rangle$, $\beta = \langle\sigma_3\rangle$, $\tilde{\pi} = \pi + \int[U - \beta'U - (\alpha^2U')']U'\,dz$, and the prime ($'$) denotes a z derivative. Thus, for channel geometry, $d\mathbf{v}/dt$ vanishes in (4) and the remaining $\langle\sigma_i\sigma_j\rangle$ terms modify the pressure and dissipation. Comparing (2) and (6) identifies counterparts as

$$\begin{aligned} &\overline{U} = U, \qquad \partial_z\langle wu\rangle = \nu[(\alpha^2U')''' - (\beta'U)''] + p_0\,, \\ &\partial_z\langle w\boldsymbol{v}\rangle = 0, \qquad \nabla(\overline{P} + \langle w^2\rangle) = \nabla(\tilde{\pi} - p_0x)\,, \end{aligned} \tag{7}$$

for a constant p_0. Using the boundary condition and reflection symmetry in this identification gives

$$\begin{aligned} &\langle w\boldsymbol{v}\rangle(z) = 0\,, \\ &-\langle wu\rangle(z) = -p_0z - \nu[(\alpha^2U')''(z) - (\beta'U)'(z)]\,, \end{aligned} \tag{8}$$

and leaves $\langle w^2\rangle$ undetermined up to an arbitrary function of z. A closure relation for $-\langle wu\rangle$ involving $U'''(z)$ also appears in Yoshizawa [20]; cf. also Eq. (8) of Ref. [4].

The general solution of the steady VCHE (6) with α constant and $\beta = 0$ (i.e., assuming isotropy and homogeneity throughout the channel), subject to the above boundary and symmetry conditions, is

$$U(z) = a\left[1 - \frac{\cosh(z/\alpha)}{\cosh(d/\alpha)}\right] + b\left(1 - \frac{z^2}{d^2}\right), \tag{9}$$

with constants a, b [22]. We show in [23] that any time-dependent solution of (4), such that $\mathbf{u}(z,t) = [U(z,t),0,0]^T$ with $U(z,t) = U(-z,t)$ and $U(\pm d,t) = 0$, converges exponentially in time to the solution (9) with the same mean flow and boundary shear stresses.

It is plausible to assume isotropy and homogeneity away from the walls, and to consider the case where $\alpha(z) \equiv \alpha_0 \equiv$ const and $\beta(z) \equiv 0$ only in that part of the channel $\{|z| \le d_0\}$ away from the walls, for some d_0, $0 < d_0 < d$, to be chosen appropriately. Given that α_0 is the typical size of the fluctuations away from the walls, our basic assumptions are that α_0/d is small and that $d - d_0$ is of the order α_0. In the part of the channel $|z| \le d_0$, the solution of (6) with the same symmetry property is given by a formula similar to Eq. (9),

$$U(z) = a\left[1 - \frac{\cosh(z/\alpha_0)}{\cosh(d_0/\alpha_0)}\right] + b\left(1 - \frac{z^2}{d_0^2}\right) + U(\pm d_0)\,.$$

In the lower half of the channel, the mean velocity U can be expressed in wall units using the notation $\phi(\eta) = U(z)/u_*$, $\eta = (z + d)/\ell_*$, with $\ell_* = \nu/u_* = d/R_0$. In this representation, the solution becomes

$$\phi(\eta) = \frac{a}{u_*}\left[1 - \frac{\cosh\,\xi(1 - \eta/R_0)}{\cosh\,\xi(1 - \eta_0/R_0)}\right] + \frac{b}{u_*}\left[1 - \left(\frac{1 - \eta/R_0}{1 - \eta_0/R_0}\right)^2\right] + \phi(\eta_0)\,, \tag{10}$$

for $\eta_0 \le \eta \le R_0$, where $\xi = d/\alpha$ and $\eta_0 = q_0 R_0 = (d - d_0)/\ell_* \sim \alpha_0/\ell_* = R_0/\xi$.

Using the definition of R and ϕ, we have $R = \int_0^{R_0} \phi(\eta)\, d\eta$. Hence (10) gives

$$R = \frac{a_0 R_0}{u_*}\left(1 - \frac{\tanh\,\xi(1-q_0)}{\xi(1-q_0)}\right) + \frac{2b_0 R_0}{3u_*} + \phi(\eta_0)(R_0 - \eta_0) + \int_0^{\eta_0} \phi(\eta)\, d\eta\,,$$

where $a_0 = a(1 - q_0)$ and $b_0 = b(1 - q_0)$. To complete this computation it is sufficient to approximate ϕ on $(0, \eta_0)$ by the piecewise linear function equal to η for $0 < \eta \le \eta_*$ and to $\phi_0 + (\eta - \eta_0)\phi_0'$ for $\eta_* \le \eta \le \eta_0$, where $\phi_0 = \phi(\eta_0)$, $\phi_0' = \phi'(\eta_0)$, and $\eta_* = (\phi_0 - \eta_0\phi_0')/(1 - \phi_0')$. We obtain

$$\frac{R}{R_0} \approx \frac{a_0}{u_*}\left[1 - \frac{\tanh\,\xi(1-q_0)}{\xi(1-q_0)}\right] + \frac{2b_0}{3u_*} + (1-q_0)\phi_0 - (1-\phi_0')^{-1}(\phi_0 q_0 - \tfrac{1}{2}q_0^2 R_0 \phi_0' - \tfrac{1}{2}\phi_0^2/R_0)\,, \tag{11}$$

where

$$\phi_0' = \frac{a\xi}{u_* R_0}\tanh[\xi(1-q_0)] + \frac{2b}{u_* R_0}(1-q_0)\,.$$

Using this and solving for ϕ_0, we obtain an explicit function $\phi_0 = \phi_0(q_0; R/R_0; a/u_*, b/u_*, \xi)$. Thus Eq. (10) becomes

$$\phi(\eta) = \frac{a}{u_*}\left[1 - \frac{\cosh\,\xi(1-\eta/R_0)}{\cosh\,\xi(1-\eta_0/R_0)}\right] + \frac{b}{u_*}\left[1 - \left(\frac{1-\eta/R_0}{1-\eta_0/R_0}\right)^2\right] + \phi_0\left(q_0; R, R_0; \frac{a}{u_*}, \frac{b}{u_*}, \xi\right). \tag{12}$$

All empirical data up to now suggest that there is a small range (z_1, z_2) of positions within the channel such that, for z in this range, the von Kármán log law is a good approximation to $U(z)$ for R (or R_0) large enough. This implies that, in this range, $U(z) - U(z_1)$ is a function of z/d only. It can be proven that, regardless of how narrow the range, the latter property implies via (12) that $a/u_* \approx a_* \cosh\,\xi(1-q_0)$, $b/u_* \approx b_*(1-q_0)^2$, and $\xi \approx \xi_*$ with some absolute constants a_*, b_*, and ξ_*. By comparing an experimental profile for R (or R_0) large enough with the profile given by our formula (12), we can obtain the values a_*, b_*, ξ_*, as well as the smallest value q_* for q_0. With these values, Eq. (12) becomes

$$\phi(\eta) = a_* \cosh\,\xi_*(1-q_*)\left[1 - \frac{\cosh\,\xi_*(1-\eta/R_0)}{\cosh\,\xi_*(1-q_*)}\right] + b_*(1-q_*)^2\left[1 - \left(\frac{1-\eta/R_0}{1-q_*}\right)^2\right] + \phi_0(R/R_0)\,, \tag{13}$$

where ϕ_0 is an explicit function of R/R_0 only, and $\eta_0 = q_* R_0 \le \eta \le R_0$. We note that, for large Reynolds numbers, $\phi_0(R/R_0)$ has the following asymptotic formula:

$$\phi_0(R/R_0) \sim \frac{R}{R_0} - C_0 + \frac{1}{2}q_0^2 C_0'\,,$$

where C_0 and C_0' depend only on a_*, b_*, ξ_*, and q_*. The ratio R/R_0 can be determined from the empirical drag laws. In this way, one can use our formula (13) to predict the profile of ϕ for any Reynolds numbers.

In Fig. 1 we compare our profiles with experimental data [4]. As the Reynolds numbers for these experiments are small, a/u_* and b/u_* have not reached their theoretical asymptotic values. These constants are therefore allowed to vary slightly with R_0 while holding ξ_* and q_* constant to fit the data. Figure 2 compares the corresponding experimental and theoretical Reynolds shear stresses. In Fig. 1 our theoretical mean-velocity profiles extend closer to the wall while still matching the empirical data; however, in Fig. 2 the corresponding Reynolds shear stresses do not so extend. Therefore, we take as q_* the least value that works for both.

Near the wall (i.e., in the region $0 < \eta < q_* R_0$) the hypotheses of isotropy and homogeneity in the Lagrangian fluctuations break down. Therefore, $\beta \neq 0$ and α depends on η. A heuristic argument gives $\beta \sim (\eta_0 - \eta)^2\beta_0$. To test whether our Eqs. (6) are still valid in this region, we observe that the statistical deduction of the VCHE in the channel provides the following realizability condition:

$$\beta \le \alpha \le \sqrt{\eta(2R_0 - \eta) + 2(R_0 - \eta)\beta}\,. \tag{14}$$

To check this condition we extrapolated [11] the experimental profiles in Fig. 1 into the near-wall region according to Panton [9] to obtain α from the first equation in (6). We found that the realizability condition (14) can be satisfied for an appropriate choice of β_0. Thus, our closure ansatz is consistent with Panton's results as well.

For larger Reynolds numbers, we use the experimental data for pipe flow given in Ref. [7]. We note that the only substantial difference between the mathematical treatment

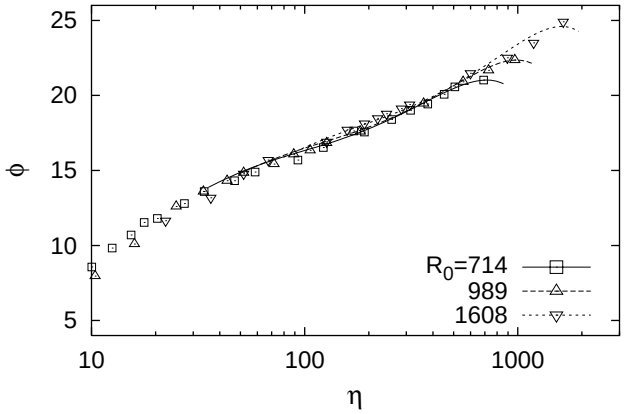

FIG. 1. The mean-velocity profile in the channel for the constant-α VCHE (represented by the solid and dashed lines) compared with the experimental data in Ref. [4].

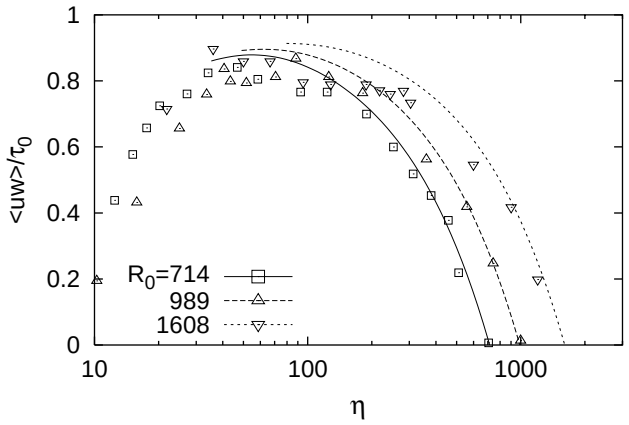

FIG. 2. Reynolds shear stress in the channel compared with the experimental data in Ref. [4].

of the two types of flows is that, for pipes, the cosh function is replaced by the first modified Bessel function I_0 (see Ref. [24]).

In Fig. 3 we compare our profiles with experimental data [7]. We obtain a_*, b_*, ξ_*, and q_* by using the experimental data for $R = 98\,812$ and then we use the von Kármán drag law for the calculation of $\phi_0(R/R_0)$ in the formula for the pipe corresponding to (13) to obtain profiles for $R = 3\,098\,100$ and $35\,259\,000$. We note that our predictions are consistent with the von Kármán log law [25] and the Barenblatt-Chorin power law [10] in the appropriate regions, as well as resolving the "chevron" near the center of the flow [26]. Our approach shows a logarithmic profile for $0.02R_0 \leq \eta \leq 0.2R_0$ and a chevron near the center of the pipe. The Barenblatt-Chorin power law [10] may represent the transition in the profile from the log law to the chevron. Moreover, the chevron is due to $b_* \neq 0$ and may reflect the fact that

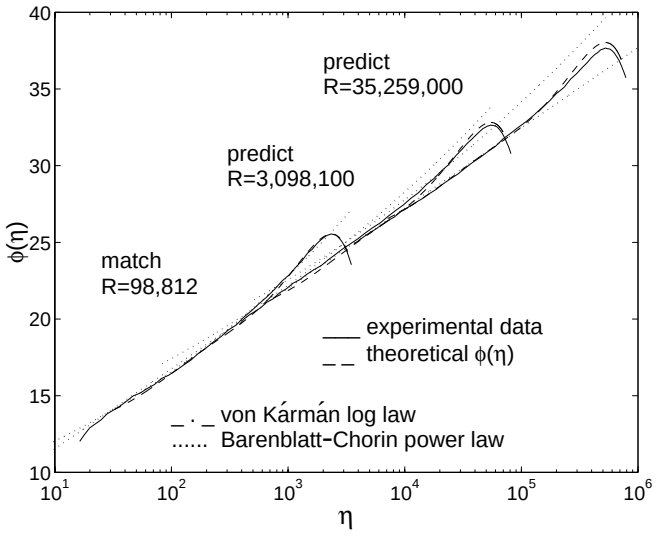

FIG. 3. The mean-velocity profile in the pipe for the constant-α viscous Camassa-Holm equation compared with the experimental data of Zagarola [7].

the Poiseuille-Hagen flow is recurrent on the attractor of the Navier-Stokes equation.

We are grateful to R. Kraichnan, K. R. Sreenivasan, and P. Constantin for constructive comments, and to D. Cioranescu for pointing out the relation between the Camassa-Holm equations and the second-grade fluids.

[1] H. Reichhardt, Naturwissenschaften **24/25**, 404 (1938).
[2] H. Eckelmann, Mitteilungen aus dem Max Planck Institut, Göttingen Report No. 48, 1970.
[3] H. Eckelmann, J. Fluid Mech. **65**, 439 (1974).
[4] T. Wei and W. W. Willmarth, J. Fluid Mech. **204**, 57 (1989).
[5] R. A. Antonia, M. Teitel, J. Kim, and L. W. B. Browne, J. Fluid Mech. **236**, 579 (1992).
[6] J. Kim, P. Moin, and R. Moser, J. Fluid Mech. **177**, 133 (1987).
[7] M. V. Zagarola, Ph.D. thesis, Princeton University, 1996.
[8] J. O. Hinze, *Turbulence* (McGraw-Hill, New York, 1975), 2nd ed.
[9] R. L. Panton, J. Fluids Eng. **119**, 325 (1997).
[10] See, e.g., G. I. Barenblatt, A. J. Chorin, and V. M. Prostokishin, Appl. Mech. Rev. **50**, 413 (1997) for a recent survey of pipe flows, and G. I. Barenblatt and A. J. Chorin, SIAM Rev. **40**, No. 2, 265 (1998).
[11] S. Chen, C. Foias, D. Holm, E. Olson, E. S. Titi, and S. Wynne, Phys. Fluids (to be published).
[12] A. A. Townsend, *The Structure of Turbulent Flow* (Cambridge University Press, Cambridge, England, 1967).
[13] D. D. Holm, J. E. Marsden, and T. S. Ratiu, Phys. Rev. Lett. **80**, 4173 (1998).
[14] R. Camassa and D. D. Holm, Phys. Rev. Lett. **71**, 1661 (1993).
[15] J. E. Dunn and R. L. Fosdick, Arch. Ration. Mech. Anal. **56**, 191 (1974).
[16] J. E. Dunn and K. R. Rajagopal, Int. J. Eng. Sci. **33**, 689 (1995).
[17] R. S. Rivlin, Q. Appl. Math. **15**, 212 (1957).
[18] A. J. Chorin, Phys. Rev. Lett. **60**, 1947 (1988).
[19] T. H. Shih, J. Zhu, and J. L. Lumley, Comput. Methods Appl. Mech. Eng. **125**, 287 (1995).
[20] A. Yoshizawa, Phys. Fluids **27**, 1377 (1984).
[21] R. Rubinstein and J. M. Barton, Phys. Fluids A **2**, 1472 (1990).
[22] With the *antisymmetric* steady solution, one may address turbulent states of Couette flow by a similar analysis.
[23] In fact, the time-dependent VCHE in a periodic box has unique classical solutions and a global attractor, whose fractal dimension is finite and scales according to Kolmogorov's estimate, $N \sim (L/\ell_d)^3$, where $\ell_d = (\nu^3/\epsilon)^{1/4}$ is the Kolmogorov dissipation length [27].
[24] M. Abramowitz and I. A. Stegun, *Handbook of Mathematical Functions* (Dover, New York, 1972), 9th ed.
[25] L. D. Landau and E. M. Lifshitz, *Fluid Mechanics* (Pergamon, New York, 1987), 2nd ed.
[26] Although our approach is in good agreement with the experiments [7], we note that in [10] it is argued that those experimental mean-velocity profiles are too low for high Reynolds numbers.
[27] C. Foias, D. D. Holm, and E. S. Titi (to be published).